Carrier effects on Raman spectra from ZnSe/GaAs heterostructures

2002 J. Phys.: Condens. Matter 14 5419

(http://iopscience.iop.org/0953-8984/14/21/316)

INSTITUTE OF PHYSICS PUBLISHING JOURNAL OF PHYSICS: CONDENSED MATTER

J. Phys.: Condens. Matter **14** (2002) 5419–5431 PII: S0953-8984(02)32878-9

Carrier effects on Raman spectra from ZnSe/GaAs heterostructures

F J Wang, D Huang, X J Wang, X X Gu and G C Yu

Surface Physics Laboratory and Department of Physics, Fudan University, Shanghai 200433, China

Received 21 January 2002, in final form 13 March 2002
Published 16 May 2002
Online at stacks.iop.org/JPhysCM/14/5419

Abstract

Non-resonant micro-Raman spectra from heterostructures of ZnSe on semi-insulating (SI-), n^+-, and p^+-GaAs using various excitation densities are reported. The effects of the carriers generated by both doping and photo-excitation have been investigated and the results are compared with those from bare GaAs substrates. The scattering from unscreened longitudinal optical phonons and coupled phonon–plasma modes in GaAs are observed in all three types of sample, but with different characteristics. The plasma was found to be electron gas in n^+-GaAs but hole gas in SI- and p^+-GaAs. Depending on the type of substrate and the density of excitation, the plasma effects induced by doping and photo-excitation in the surface and in the deeper regions are demonstrated. As compared to the case for bare GaAs substrates, the density of photo-carriers generated by a given excitation was significantly enhanced in ZnSe/GaAs heterostructures, demonstrating a longer lifetime and a lower recombination rate of photo-carriers in the latter type of structure. The band diagrams of the ZnSe/GaAs heterojunctions in all three cases were obtained from the Raman spectra. In contrast to the carrier effects, no electric field-induced scattering was observed in forbidden configurations.

1. Introduction

Raman spectroscopy has been extensively used to study the surfaces and interfaces of semiconductor heterostructures [1]. Depending on the properties of the semiconductor and the conditions of excitation, various Raman spectra with different scattering mechanisms can be observed. For an undoped semiconductor with a small surface band bending, the Raman spectra are similar to those from bulk crystal. For a zinc-blende structure such as GaAs, in the configuration of backscattering from the (001) surface, first-order Raman scattering is only allowed from the LO phonons when the incident and scattered light are perpendicularly polarized along ⟨100⟩ directions or polarized parallel along ⟨110⟩ directions [2]. When a semiconductor is heavily donor doped, like n^+-GaAs, two branches

of coupled phonon–plasma modes result [3]. The lower branch (L^-) is phonon-like and the energy is close to that of the TO phonons (screened LO phonons), while the upper branch (L^+) is plasma-like and the energy is much higher and the scattering spectrum much broader. When a semiconductor is heavily acceptor doped, like p^+-GaAs, the situation is very different [4–6]. In this case, only one coupled mode is observed (labelled as L in the following) due to high levels of plasma (hole gas) damping. The energy of the L mode shifts from unscreened to screened LO phonons as the doping density increases. All coupled modes are Raman allowed and can be observed in the same scattering configurations as for the bulk LO phonons. For many semiconductors, the LO phonons from the depletion layer and the coupled mode from deeper layers (bulk) may be observed simultaneously in the Raman spectra. From the relative intensity of the Raman spectra from the two regions, information on the surface barrier and the depletion layer can be inferred.

In addition to the allowed modes, Raman spectra in the forbidden configurations have been reported for the depletion layer near the semiconductor surface [1]. There are considered to be two mechanisms of scattering: the electric field-induced scattering [7] and the scattering at finite wavevectors activated by impurities or strong absorption. The intensity of forbidden scattering is very weak in non-resonant excitation but dramatically enhanced by resonant excitation. These modes are of great interest in the investigation of scattering mechanisms as well as semiconductor materials.

The surface properties can be modified by strong laser excitation at energies beyond the fundamental gap [8]. Unlike the case of the carriers created by doping, the carriers generated by laser excitation contain both electrons and holes. Both may couple with LO phonons to form coupled modes. Therefore it is, in principle, a multiple-coupled-mode system. Due to the surface field and the different lifetimes of electrons and holes, the densities of electrons and holes and their distributions under continuous-wave (cw) excitation may be very different in various materials. As a result, the Raman spectra under different excitations contain detailed information on the surface and the bulk properties of semiconductors.

The properties of semiconductors are also modified when the surface is covered by some other materials. Among various material systems, the ZnSe/GaAs heterostructure is particularly interesting due to its applications in optoelectronic devices. This system is also well suited for the investigation of the various mechanisms of light scattering [9–13]. In this system, high-quality crystals can be grown due to the small lattice mismatch between ZnSe and GaAs. ZnSe has a much higher band gap (2.7 eV) than GaAs (1.4 eV); so the visible light used in the light scattering experiments can penetrate the ZnSe epilayer and easily probe the ZnSe/GaAs heterojunction. In addition, bulk phonon modes in the two materials have different energies and are well separated in the Raman spectra. The band alignment at the interface is well understood and the band offset is mainly distributed in the valence band. Although this system has been extensively investigated, there are still some important questions, mainly related to the complications of the interfaces, which have not been clearly answered. For example, is the Fermi level pinned at the interface? What are the band diagrams of the heterojunctions? How do the photo-carriers transfer across the interface and affect the optical properties of the structure? And what are the effects of the interface defects and the misfit dislocations on the carrier generation and recombination?

It is the purpose of this investigation to address some of the questions listed above. The main concern is the carrier effects on the Raman spectra and the band diagram of ZnSe/GaAs heterostructures. Three types of GaAs were used: semi-insulating (SI-), n^+-, and p^+-type. Micro-Raman spectra were measured under various excitation densities to examine the effect of both doping and photo-carriers and to obtain information on the band diagrams of the materials.

2. Experiment

The samples used in this investigation were nominally undoped ZnSe films grown on SI-, n^+-, and p^+-GaAs(001) substrates by molecular beam epitaxy (MBE). The bare SI-, n^+-, and p^+-GaAs substrates were also used for comparison. The doping concentration was $\sim 2 \times 10^{18}$ cm^{-3} in n^+-GaAs and $\sim 1 \times 10^{19}$ cm^{-3} in p^+-GaAs. In the case of SI-GaAs, the samples are n-type [14] with electron concentrations at room temperature of the order of $\sim 10^9$ cm^{-3}. Before MBE growth, the GaAs substrates were cleaned in $5H_2SO_4$:$1H_2O_2$:$1H_2O$ solution, rinsed in deionized water, and thermally deoxidized at $\sim$580 °C in the growth chamber. During the growth of ZnSe films, the growth temperature was 350 °C. The ZnSe films have a typical thickness of ~ 0.5 μm and show n-type background doping with a density of $\sim 10^{16}$ cm^{-3}.

Micro-Raman measurements were performed using a Renishaw 2000 set-up at room temperature. The excitation source is the 514.5 nm line from a cw Ar^+ laser. The maximum laser intensity on the sample surface is $\sim$4 mW and the laser beam was focused to a spot with a diameter of ~ 2 μm resulting in the maximum excitation density $\sim$100 kW cm^{-2}. Under this excitation, photo-carriers with densities higher than 10^{18} cm^{-3} can be generated in GaAs as will be discussed later. The excitation density can be changed by using neutral density filters. Both allowed and forbidden spectra in the backscattering configuration were measured by using appropriate polarizers and waveplates, and the Raman signal was detected by a charge-coupled-device (CCD) detector. Conventional Raman spectroscopy was also performed using a 1 m double monochromator (Jobin-Yvon U1000), using two different excitation wavelengths: 488.0 and 514.5 nm.

The ZnSe film is transparent to the excitation wavelength of 514.5 nm. For GaAs, this wavelength is far from any electronic resonance. The penetration depth of the laser beam in GaAs [15] is $\sim$100 nm and the Raman probe depth is $\sim$50 nm. Therefore, the Raman spectra can probe both the depletion region and the bulk layers in various types of GaAs and ZnSe/GaAs heterostructure.

3. Results and discussion

3.1. ZnSe on semi-insulating GaAs

Figure 1 shows the Raman spectra from SI-GaAs under four excitation densities, from 1 to 100 kW cm^{-2}. At low excitation density (spectrum a), only the scattering from unscreened LO phonons (292 cm^{-1}) is observed. The peak width (full width at half-maximum) is 3.8 cm^{-1}. With increase in excitation density, this peak becomes broader but its energy changes little. The peak width increases to 10 cm^{-1} at the highest excitation (spectrum d). The excitation dependence of the spectra shows that this peak does not arise from pure LO phonons at high excitation but from the coupled phonon–plasma mode. The plasma is due to the photo-holes as will be evident later when we analyse the line shapes as a function of carrier density. In addition to the changes in the main peak, a weak peak, at TO phonon energy (268 cm^{-1}), builds up as the excitation density increases. However, this peak cannot arise from the TO phonons since it is forbidden in this scattering configuration and not observed at low excitation. We attribute this peak to the LO phonons screened by photo-electrons as will be discussed later.

Figure 2 presents the Raman spectra from the ZnSe/SI-GaAs heterostructure at various excitation densities. In these spectra, scattering from the LO phonons in the ZnSe film was observed and found to be independent of the excitation density. A weak peak at the energy of the TO phonon in ZnSe was also evident at high excitations. As compared to the case for the bare SI-GaAs, the change in the GaAs peaks with excitation density is more significant in the

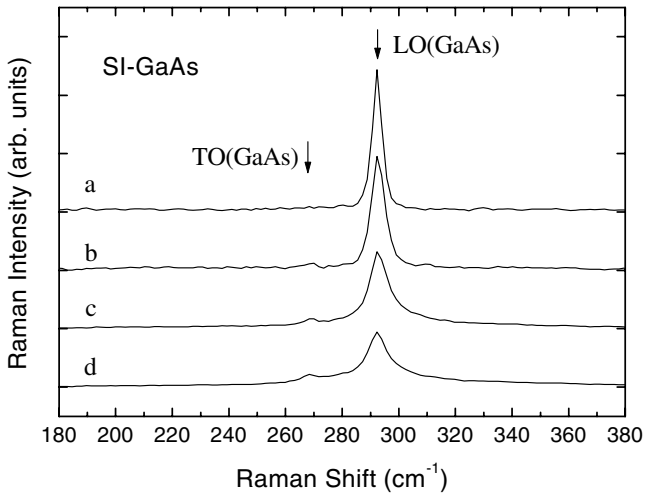

Figure 1. Raman spectra from the SI-GaAs under excitation densities of (a) 1, (b) 10, (c) 50, and (d) 100 kW cm^{-2}. The Raman intensity was reduced by a factor of 1, 10, 50, and 100 for the spectrum a, b, c, and d, respectively.

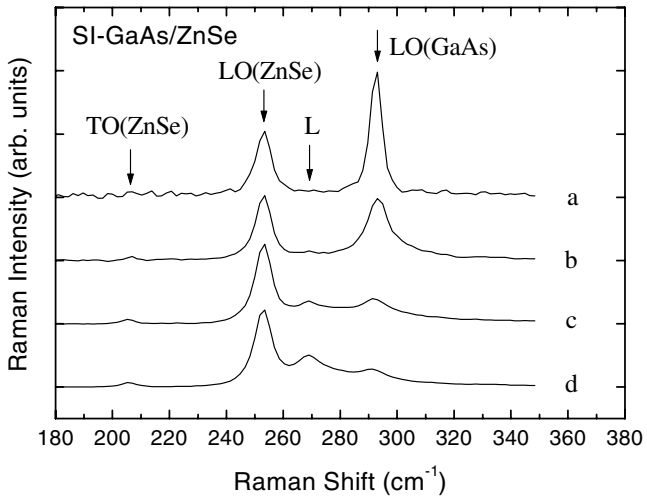

Figure 2. Raman spectra from the ZnSe/SI-GaAs heterostructure under excitation densities of (a) 1, (b) 10, (c) 50, and (d) 100 kW cm^{-2}. The Raman intensity was reduced by a factor of 1, 10, 50, and 100 for the spectrum a, b, c, and d, respectively.

ZnSe/SI-GaAs heterostructure. The result suggests a much higher carrier population near the ZnSe/SI-GaAs interface than that near the SI-GaAs surface generated by the same excitation density. In the SI-GaAs, under the highest excitation (spectrum d), the plasma density is still low and the coupled mode is at an energy near 292 cm^{-1}. In the ZnSe/SI-GaAs heterostructure under the same excitation, however, the plasma density is much higher and the coupled mode shifts to $\sim$268 cm^{-1}, approaching a screened LO mode.

These Raman spectra were only observed in the allowed configurations. No scattering was observed in forbidden configurations at different excitation densities. Therefore, both field-induced scattering and the finite-wavevector-induced scattering are negligible in this case, in

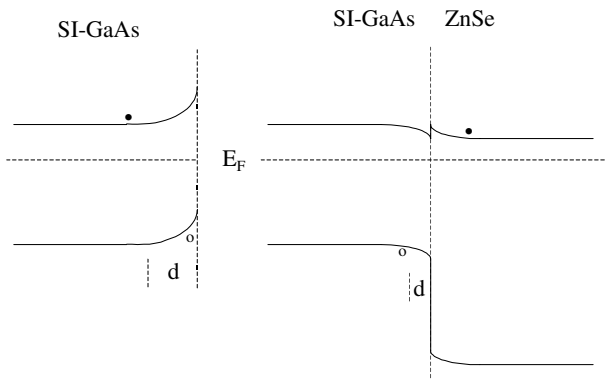

Figure 3. Band diagrams of the SI-GaAs and the ZnSe/SI-GaAs heterostructure. The photo-electrons and holes are schematically shown by solid and empty dot respectively. The depletion layer is represented by d.

contrast to those reported in [13] and [11]. The result is mainly attributed to the non-resonant excitation and the small band bending. As shown in the literature [16], the forbidden scattering is very weak at non-resonant excitation and can be enhanced by a few orders of magnitude when the laser energy approaches the resonant energy.

According to the material properties and the measured Raman spectra, the band diagrams for the SI-GaAs and ZnSe/SI-GaAs heterojunctions at low excitation are presented in figure 3. For the SI-GaAs, the Fermi level at the surface was pinned near the mid-gap. An upward band bending is established, similar to that for n-type GaAs [14]. Photo-excitation causes an accumulation of the holes near the surface but the photo-electrons are swept into the bulk by the surface field. For ZnSe/SI-GaAs, the Fermi level is no longer pinned at the interface. In this case, due to the different doping concentrations across the interface, a downward band bending is produced in the GaAs. The photo-electrons created in GaAs are easily swept into the ZnSe layer while the photo-holes remain in the GaAs bulk and couple to the LO phonons.

The scattering from the coupled phonon–plasma mode due to the photo-holes was confirmed by the calculated Raman spectra, shown in figure 4. We used the dielectric model of Hon and Faust [4] that was first used for GaP and then developed by Mlayah *et al* [6] for p-GaAs bulk crystals. Within this dielectric approach, by taking into account both the allowed deformation potential and the electro-optic contribution, the rate of Stokes Raman scattering by the LO phonon-damped plasmon mode in the long-wavelength limit can be written as [6]

$$I_s(\omega) = \frac{A\omega\Gamma_P\omega_P^2[\omega_T^2(1+C)-\omega^2]^2}{D},$$

with

$$D = [\omega^2(\omega_L^2-\omega^2)-\omega_P^2(\omega_T^2-\omega^2)+\gamma\Gamma_P\omega^2]^2 + [\Gamma_P\omega(\omega_L^2-\omega^2)+\gamma\omega(\omega_P^2-\omega^2)]^2,$$

where A is an ω-independent factor, C is the Faust–Henry coefficient, ω_{TO} is the frequency of the TO phonons, ω_{LO} and γ are the frequency and damping constant of the LO phonons respectively, and ω_P and Γ_P are the frequency and damping constant of the plasma respectively. The data used in the calculations are: $C = -0.57$ [17], $\omega_{TO} = 268$ cm^{-1}, $\omega_{LO} = 292$ cm^{-1}, $\gamma = 2.0$ cm^{-1}, $\Gamma_P = 550$ cm^{-1}. Only the plasma frequency was changed according to the excitation density: $\omega_P \sim p^{1/2} \sim I_{laser}^{1/2}$. The values used are 70, 200, 450, and 630 cm^{-1} for spectra a, b, c, and d, respectively.

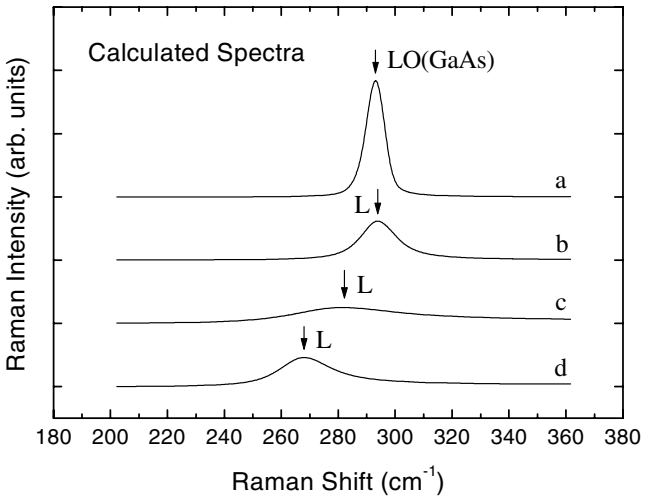

Figure 4. The calculated Raman spectra from coupled phonon–plasma mode with large plasma damping. The parameters used in the calculations are: $C = -0.57$, $\omega_{LO} = 292$ cm^{-1}, $\omega_{TO} = 268$ cm^{-1}, $\gamma = 2.0$ cm^{-1}, $\Gamma_p = 550$ cm^{-1}. The plasma frequency is 70, 200, 450, and 630 cm^{-1} for the spectrum a, b, c, and d, respectively.

The calculated spectra can be directly compared to the measured results shown in figure 2. A detailed comparison between the measured (figure 2) and the calculated (figure 4) spectra shows that the peak at 292 cm^{-1} contains contributions from both unscreened LO phonons and the coupled mode. The former is from the interface depletion layer; as the measured spectra show, the scattering from the unscreened LO phonons is observed even under the highest excitation. As compared to the case for the ZnSe/SI-GaAs heterojunction, the holes are accumulated nearer the surface in bare SI-GaAs and have a much lower density due to a high rate of surface recombination. In addition to that of the holes, the effect of the photo-electrons is observed, as a weak peak from the screened LO phonons in the bulk near 268 cm^{-1} at high excitation.

3.2. ZnSe on n$^+$-type GaAs

Figure 5 presents the Raman spectra from the bare n$^+$-GaAs measured at different excitation densities. Both unscreened LO phonon and plasma–phonon coupled modes are observed. The energy of the L$^-$mode is 268 cm^{-1} and changes little with the excitation density. The L$^+$ mode at low excitation was observed at 510 cm^{-1} and increases a little (by $\sim$10 cm^{-1}) at the high excitation density. From the latter peak, the electron density is obtained [3] as 2.5×10^{18} cm^{-3}, consistent with the doping concentration.

The Raman spectra with different laser wavelengths show that the unscreened LO peak is from the depletion layer near the surface and the coupled modes at the TO energy are from the bulk. The contributions from the two regions to the scattering spectra are comparable at low excitation. For GaAs with $n \approx 2 \times 10^{18}$ cm^{-3}, assuming the Fermi level at the surface to be pinned at mid-gap, the thickness of the depletion layer is calculated to be 25 nm, about half of the Raman probe depth. This accounts for the similar intensities of the LO and the coupled modes observed in the spectra. With increasing excitation density, the LO peak loses intensity, while the L$^+$ mode only shifts a little. These observations demonstrate that the main effect of the photo-carrier in this case is the reduction of the depletion layer width rather than

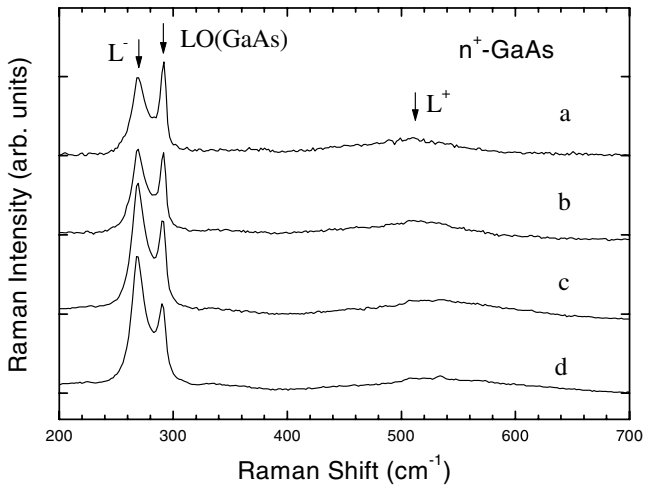

Figure 5. Raman spectra from the n^+-GaAs under excitation densities of (a) 1, (b) 10, (c) 50, and (d) 100 kW cm^{-2}. The Raman intensity was reduced by a factor of 1, 10, 50, and 100 for the spectrum a, b, c, and d, respectively.

the increase in the electron concentration in the bulk. The Raman scattering with different polarizations shows that the spectra are only observed at allowed configurations, suggesting that the electric field-induced scattering is negligible.

Figure 6 shows the Raman spectra from the ZnSe/n^+-GaAs heterostructure under various excitation densities. Similar to what we observed for the ZnSe/SI-GaAs sample, the growth of ZnSe film on n^+-GaAs significantly enhances the population of photo-carriers and reduces the width of the depletion layer. At the highest excitation, the unscreened LO peak from GaAs almost disappears. In addition, the L^+ peak shifts to higher energy by more than 100 cm^{-1}. These results demonstrate that, under this excitation, not only does the depletion layer disappear but also the electron population is increased significantly. From the changes in the L^+ peaks, an increase in the electron density from 2.5×10^{18} to 4.0×10^{18} cm^{-3} is obtained, corresponding to a density of photo-electrons of $n_p \sim 2 \times 10^{18}$ cm^{-3}. From the density of photo-electrons (n_p), the excitation density I_i, and the absorption length l_a of the incident laser, the electron lifetime is obtained from $\tau = n_p l_a/(I_i/h\nu)$ as ~0.1 ns. It is clear that the electron lifetime in n^+-GaAs is significantly increased by the growth of ZnSe films. Even though the misfit dislocations appear near the ZnSe/GaAs interface, the surface recombination rate of the excess carriers is still lower than that in the bare n^+-GaAs surface.

Band diagrams consistent with the Raman spectra for n^+-GaAs and ZnSe/n^+-GaAs heterostructure at low excitation density are shown in figure 7. In the bare n^+-GaAs, the Fermi level at the surface is pinned near mid-gap [18]. Two essential changes are observed on growing ZnSe on n^+-GaAs:

(1) The depletion width is much reduced since the Fermi level is no longer pinned at the interface.
(2) The electron density is significantly increased under the same excitation due to a lower interface recombination rate.

The first change leads to intensity reduction of the unscreened LO peak from the depletion layer. The second change shifts the coupled mode L^+ to a higher energy. It should be emphasized that the density of holes near the n^+-GaAs surface is much lower than that of electrons due to

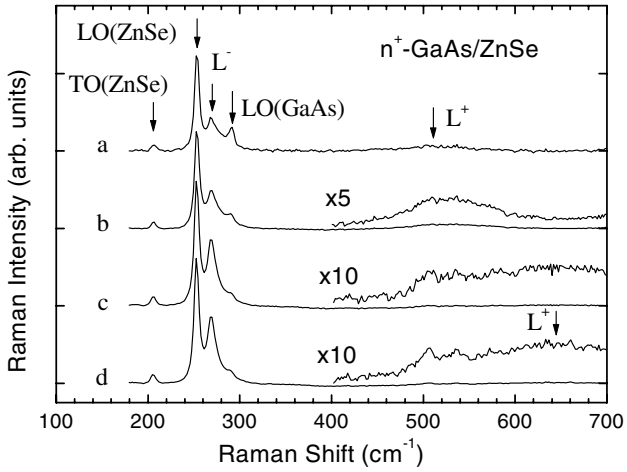

Figure 6. Raman spectra from the ZnSe/n$^+$-GaAs heterostructure under excitation densities of (a) 1, (b) 10, (c) 50, and (d) 100 kW cm^{-2}. The Raman intensity was reduced by a factor of 1, 10, 50, and 100 for the spectrum a, b, c, and d, respectively.

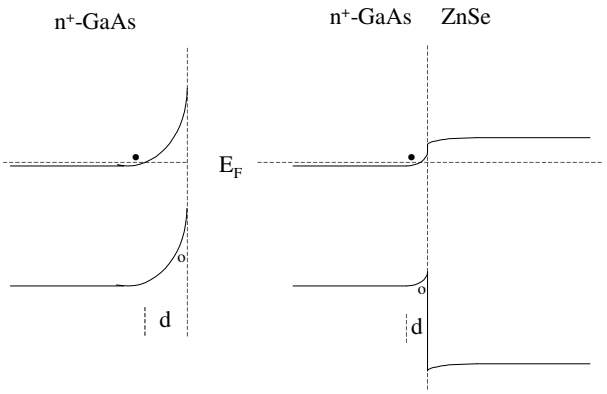

Figure 7. Band diagrams of the n$^+$-GaAs and ZnSe/n$^+$-GaAs heterostructure. The photo-electrons and holes are schematically shown by solid and empty dot respectively. The depletion layer is represented by d.

the surface recombination. In the ZnSe/n$^+$-GaAs heterostructure, the hole density is also much lower than the electron density since the holes can be captured by the defect states in ZnSe, which may be induced by atomic inter-diffusion or by misfit dislocations. As we observed [19], the defect states in ZnSe near the interface are of acceptor type and have energies not far from the valence band in the GaAs.

Quantitative analysis of the Raman spectra from the coupled L^- and L^+ modes was carried out. For the allowed deformation potential and electro-optic contributions, it has been shown that the Raman scattering efficiency is given by [1, 20]

$$\frac{\mathrm{d}^2\sigma}{\mathrm{d}\Omega\,\mathrm{d}\omega} \propto \left(\frac{\omega_T^2(1+C)-\omega^2}{\omega_T^2-\omega^2}\right)^2 \mathrm{Im}\left(-\frac{1}{\varepsilon}\right),$$

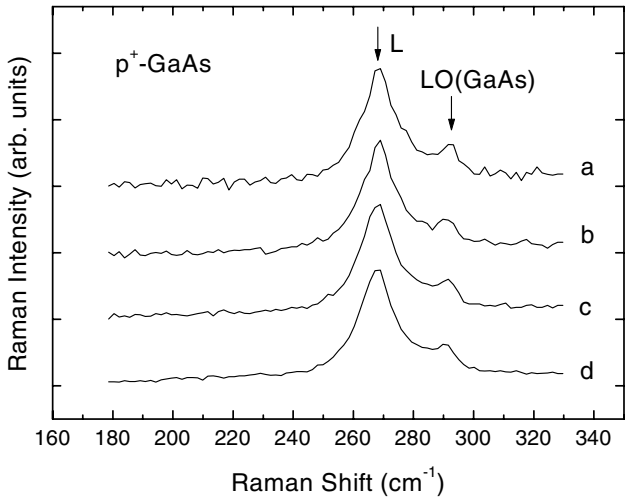

Figure 8. Raman spectra from the p^+-GaAs under excitation densities of (a) 1, (b) 10, (c) 50, and (d) 100 kW cm^{-2}. The Raman intensity was reduced by a factor of 1, 10, 50, and 100 for the spectrum a, b, c, and d, respectively.

where ε is the total dielectric constant:

$$\varepsilon = \frac{\omega_L^2 - \omega_T^2}{\omega_T^2 - \omega^2} + \varepsilon_e.$$

ε_e includes the effect of the phonon–plasmon coupling which is given by the Lindhard–Mermin function [21]. The quantitative calculations of the Raman spectra confirm the origin of the peak. By comparing the calculated and the measured spectra and the intensity changes of the LO and coupled modes with laser excitation, the modulation of the band bending by the laser excitation was obtained in both n^+-GaAs and ZnSe/n^+-GaAs heterostructure. The main result is that the band bending near the n^+-GaAs surface, shown in figure 7, is reduced by ∼60% under excitation of 100 kW cm^{-2}. For the ZnSe/n^+-GaAs heterojunction, the band bending is almost totally removed under the same excitation. Further details of these aspects will be reported elsewhere.

3.3. ZnSe on p^+-type GaAs

Figure 8 shows the Raman spectra from the p^+-GaAs under different excitation densities. Unlike those from SI- and n^+-GaAs, the spectra from p^+-GaAs are essentially independent of the excitation density. The main peak is from the damped plasma–phonon coupled mode as discussed earlier. Due to the high density of holes in the bulk, the LO phonons were fully screened by the holes and shifted to 268 cm^{-1}. The weak peak at 292 cm^{-1} is from the unscreened LO phonons in the depletion layer which is only ∼10 nm due to the high level of doping ($N_A \sim 1 \times 10^{19}$ cm^{-3}). As we showed in the last subsection, the density of the photo-carriers under 100 kW cm^{-1} excitation is $\sim 2 \times 10^{18}$ cm^{-3} in the ZnSe/n^+-GaAs heterojunction but lower in the bare n^+-GaAs. This density is much lower than the doping concentration in the p^+-GaAs, resulting in a negligible contribution to the Raman spectra. The plasma frequency, $\omega_P = (4\pi ne^2/m^*)^{1/2}$, in p^+-GaAs is nearly the same as that in n^+-GaAs (∼510 cm^{-1}) since the carrier density (1×10^{19} cm^{-3} as compared to 2×10^{18} cm^{-3}) and the effective mass ($0.34m_0$ as compared to $0.067m_0$) are both increased by a factor of five. As the calculated

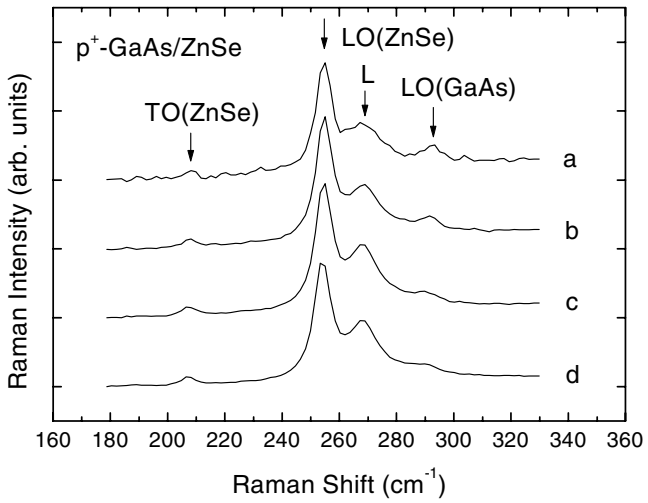

Figure 9. Raman spectra from the ZnSe/p^+-GaAs heterostructure under excitation densities of (a) 1, (b) 10, (c) 50, and (d) 100 kW cm^{-2}. The Raman intensity was reduced by a factor of 1, 10, 50, and 100 for the spectrum a, b, c, and d, respectively.

spectra show in the figure 4, a hole gas at $\sim 1 \times 10^{19}$ cm^{-3} and of plasma frequency >500 cm^{-1} should screen the LO phonons well and bring the coupled mode to the position of ~ 268 cm^{-1}. As expected, only one coupled mode was observed due to the high level of plasma damping.

Figure 9 shows the Raman spectra from the ZnSe/p^+-GaAs heterostructure under different excitation densities. Again, all spectra were obtained in the allowed configuration. No forbidden scattering was observed. Similarly to the cases of SI- and n^+-GaAs, the growth of ZnSe again enhances the effect of photo-excitation on the GaAs spectra. With the increase in the excitation density, a decrease in the LO phonon scattering is observed due to the reduction in the depletion layer width. The hole density increase in the bulk is also noticeable from the spectral changes of the coupled mode.

Figure 10 presents the band diagrams of p^+-GaAs and ZnSe/p^+-GaAs heterostructure under low excitation. These diagrams are consistent with the measured Raman spectra. Fermi-level pinning near the mid-gap is assumed at the bare p^+-GaAs surface [22]. In both cases, the electron population in GaAs by laser excitation is very low due to the high level of surface recombination in the bare p^+-GaAs and due to the sweeping of the electrons to the ZnSe by the built-in field in the ZnSe/p^+-GaAs heterojunction.

The origin of the Raman peaks from the depletion layers and the bulk at low excitation was confirmed by the conventional Raman spectra using different laser wavelengths. The modulation of the band bending by high laser excitation was also derived for the ZnSe/p^+-GaAs heterojunction from the Raman spectra.

3.4. Discussions

All of the Raman spectra were observed in the allowed scattering configuration. No forbidden scattering such as electric field-induced scattering was detectable, showing a negligible effect of electric field on the Raman spectra in this investigation. The band diagrams of ZnSe/GaAs heterostructures compatible with the Raman spectra and the band discontinuities also do not favour Fermi-level pinning at the heterointerfaces, in contrast to recent reports [13].

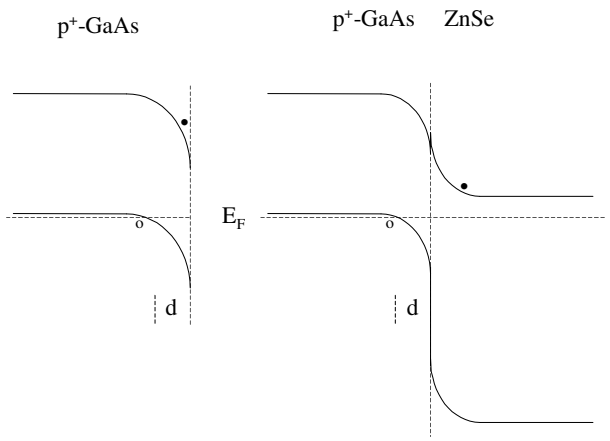

Figure 10. Band diagrams of the p^+-GaAs and the ZnSe/p^+-GaAs heterostructure. The photo-electrons and holes are schematically shown by solid and empty dot respectively. The depletion layer is represented by d.

The negligible effect of electric field and non-pinning of the Fermi level in the ZnSe/GaAs heterostructures used in this study are essentially due to low interface densities of dangling bonds generated by the dislocations and the higher interface quality [10]. The high quality of the ZnSe/GaAs heterostructures was also demonstrated by the sharp exciton–polariton spectra from similar ZnSe films [19].

In the analysis of the Raman spectra, a single-component homogeneous plasma has been assumed either in the surface region or in the region beneath the depletion layer. The single-component description is justified since the photo-electrons and holes are swept in opposite directions due to the band bending near the GaAs surface or the ZnSe/GaAs interface, as presented in figures 3, 7, and 10. The inhomogeneous carrier distribution due to the diffusion and the surface recombination may affect the Raman spectra. As shown in [23], the inhomogeneous distribution of the carriers may produce peak energy of the coupled mode insensitive to the excitation density. However, later investigations reported in the literature attribute similar spectra to the large damping of plasma caused by holes rather than carrier inhomogeneity [5, 6, 17]. For the SI-GaAs and ZnSe/SI-GaAs used in this study, the hole nature of the coupled mode is evident not only from the band diagram (figure 3), but also on comparing the measured Raman spectra to the calculated results (figure 4) and to those obtained for p^+-GaAs (figures 8 and 9). Therefore the main characteristics of the Raman spectra are determined by the plasma damping rather than the plasma inhomogeneity.

We finally comment that the Raman spectra from ZnSe/GaAs heterostructures at different excitation density contain rich information on the materials. On one hand, due to the small lattice mismatch between the ZnSe/GaAs and the low dislocation densities near the interface, the surface recombination rate is dramatically reduced when the GaAs is covered by ZnSe film, as shown in the Raman spectra. On the other hand, due to the small conduction band offset, the photo-created electrons in the GaAs may easily transfer to the ZnSe while the photo-holes remain in the GaAs layer (see figures 3 and 10). This is in contrast to the case for AlGaAs/GaAs materials in which both electrons and holes may be well confined in the GaAs layer [24]. The low rate of interface recombination and the special mode of carrier transfer may lead to interesting non-linear optical properties. More quantitative information of the carrier effect on the band structures can be obtained by a more detailed analysis of the Raman spectra.

4. Conclusions

Non-resonant micro-Raman spectra have been obtained from the heterostructures of ZnSe on SI-, n^+-, and p^+-GaAs, under various excitation densities. The effects of carriers induced by both doping and photo-excitation were investigated and the results were compared to those from bare GaAs samples. The scattering from unscreened LO phonons and coupled phonon–plasma modes in GaAs are observed in all three cases, but with different characteristics. For the SI-GaAs and the ZnSe/SI-GaAs heterostructure, the plasma consists mainly of holes generated by laser excitation and located in different regions. In the bare SI-GaAs, the holes are accumulated near the surface, while the electrons are located in the deeper layers. The unscreened LO mode dominates the low-excitation spectra and the coupled mode dominates the high-excitation spectra. In the case of the ZnSe/SI-GaAs heterostructure, the holes are generated in the GaAs bulk and the dependence of the Raman spectra on excitation density is more significant. When the excitation density changes from 1 to 100 kW cm^{-2}, the energy of the coupled mode shifts from that of the unscreened to that of the screened LO mode. For the n^+-GaAs and the ZnSe/n^+-GaAs heterostructure, the plasma consists of the electrons from doping, at low excitation. With the increase in excitation density, the contribution from photo-carriers is observed. In the bare n^+-GaAs, the effect is mainly the reduction in the depletion layer width. In the ZnSe/n^+-GaAs heterostructure, both reduction in the depletion layer width and increase in the bulk electron density are observed. For the p^+-GaAs and the ZnSe/p^+-GaAs heterostructure, the plasma consists of holes, mainly from the doping. The effect of photo-carriers is only observed in the ZnSe/p^+-GaAs heterostructure where the narrowing of the depletion layer and the increase in the bulk hole density are observed under high excitation. From the measured Raman spectra, the band diagrams of the ZnSe/GaAs heterostructures in all three cases are inferred, and the Fermi levels at the ZnSe/GaAs interfaces are not pinned. As compared to the case for bare GaAs, the lifetime of the photo-carriers in the ZnSe/GaAs heterostructures is significantly increased. No contribution of forbidden scattering induced by an electric field or activated by impurities or strong absorption has been observed.

Acknowledgment

This work was supported by the National Natural Science Foundation of China.

References

[1] Abstreiter G, Cardona M and Pinczuk A 1984 *Light Scattering in Solids* vol 4, ed M Cardona and G Güntherodt (Berlin: Springer) p 107
[2] Cardona M 1982 *Light Scattering in Solids* vol 2, ed M Cardona and G Güntherodt (Berlin: Springer) p 49
[3] Klein M V 1983 *Light Scattering in Solids* vol 1, ed M Cardona (Berlin: Springer) p 155
[4] Hon D T and Faust W L 1973 *Appl. Phys.* **1** 241
[5] Wan K and Young J F 1990 *Phys. Rev.* B **41** 10 772
[6] Mlayah A, Carles R, Landa G, Bedel E and Munoz-Yague A 1991 *J. Appl. Phys.* **69** 4064
[7] Pinczuk A and Burstein E 1968 *Phys. Rev. Lett.* **21** 1073
[8] Romanek K M, Nather H and Göbel E O 1981 *Solid State Commun.* **39** 23
[9] Walsh D, Mazuruk K and Benzaquen M 1987 *Phys. Rev.* B **36** 2883
[10] Olego D J 1987 *Appl. Phys. Lett.* **51** 1422
Olego D J 1989 *Phys. Rev.* B **39** 12 743
[11] Talaat H, Elissa L, Negm S, Burstein E, Yeganeh M S and Yodh A G 1994 *J. Vac. Sci. Technol.* B **12** 2598
[12] Ichimura M, Usami A, Wada T, Fujita S and Fujita S 1993 *Appl. Phys. Lett.* **62** 1800
[13] Pagés O, Renucci M A, Briot O and Aulombard R L 1996 *J. Appl. Phys.* **80** 1128
Pagés O, Renucci M A, Briot O and Aulombard R L 1999 *J. Appl. Phys.* **85** 2371

[14] Yin X, Guo X X, Pollak F H, Pettit G D, Woodall J M, Chin T P and Tu C W 1992 *Appl. Phys. Lett.* **60** 1336
[15] Shen H and Pollak F H 1985 *Appl. Phys. Lett.* **47** 891
[16] Abstreiter G, Cardona M and Pinczuk A 1984 *Light Scattering in Solids* vol 4, ed M Cardona and G Güntherodt (Berlin: Springer) p 111
[17] Pages O, Renucci M A, Briot O and Aulombard R L 1995 *J. Appl. Phys.* **77** 1241
[18] Sze S M 1981 *Physics of Semiconductor Devices* (New York: Wiley)
[19] Wang X J, Huang D, Sheng C X and Yu G C 2001 *J. Appl. Phys.* **90** 6114
[20] Abstreiter G, Trommer R, Cardona M and Pinczuk A 1979 *Solid State Commun.* **30** 703
[21] Mermin N D 1970 *Phys. Rev.* B **1** 2362
[22] Spiter W G and Mead C 1963 *J. Appl. Phys.* **34** 3061
[23] Young J F, Wan K, SpringThorpe A J and Mandeville P 1987 *Phys. Rev.* B **36** 1316
[24] Pinczuk A, Shah J and Wolff P A 1981 *Phys. Rev. Lett.* **47** 1487